Signal Processing: Image Communication 68 (2018) 120–128

Contents lists available at ScienceDirect

Signal Processing: Image Communication

journal homepage: www.elsevier.com/locate/image

High dynamic range image tone mapping based on asymmetric model of retinal adaptation

Dae-Hong Lee, Ming Fan, Seung-Wook Kim, Mun-Cheon Kang, Sung-Jea Ko *

Department of Electrical Engineering, Korea University, Republic of Korea

ARTICLE INFO

Keywords:
High dynamic range image
Tone mapping operator
Retina response model
Perceptual image processing

ABSTRACT

Global tone mapping operators using the symmetrical retinal response model to light tend to produce a low dynamic range (LDR) image that exhibits loss of details of its corresponding high dynamic range (HDR) image in a bright or dark area. In this paper, we introduce a new asymmetric sigmoid curve (ASC) based on the model of retinal adaptation encompassing symmetrical S-shaped curve, and present two global tone mapping operators by using the ASC. In the proposed method, an ASC-based tone mapping function is obtained by using a well-known classic photography technique, called zone system. In addition, a contrast-enhancing tone mapping function is introduced by formulating a bi-criteria optimization problem with the luminance histogram of an input HDR image and the ASC-based mapping function. Experimental results demonstrate that the proposed method enhances the global contrast while preserving image details in the tone-mapped LDR image. Moreover, the objective assessment results using an image quality metric indicate that the proposed method shows a high performance to state-of-the-art global tone mapping operators.

1. Introduction

With the rapid development of high dynamic range (HDR) technology, HDR images can provide far more lightness and color information than 24-bit RGB images [1]. However, since most display devices still have a low dynamic range (LDR), various types of tone mapping operator have been proposed to represent an HDR image on LDR devices. These methods can be broadly classified into two parts: global [2–10] and local [11–19] operators.

The global tone mapping operator applies a spatially invariant compression function to each pixel to compress the dynamic range of an HDR image. For example, some quantization functions such as a gamma function or a logarithmic function are used for simply compressing the dynamic range of an HDR image [4,10]. On the other hand, the local tone mapping operator utilizes a different compression ratio at each pixel by considering the local information of neighboring pixels to preserve the details in the output images. For example, Durand et al. [17] used the local edge-preserving filter for decomposing an input HDR image into an HDR base layer and LDR detail layer. Then, only the HDR base layer is compressed and recombined with the LDR detail layer. Similarly, Fattal et al. [18] efficiently preserved the fine details of the tone-mapped LDR image by using a gradient attenuation function which compresses only the large gradient of an HDR image.

An objective [20] and a subjective [21] comparison of these two operators indicated that the global tone mapping operator reproduces the global contrast better, but results in loss of detail information. Meanwhile, the local tone mapping operator has a better detail visibility property, but is less efficient in reducing the computational complexity as compared with the global operator. In addition, the local operator tends to create unnatural appearances such as ringing and halo artifacts.

Since the human visual system (HVS) successfully deals with the dynamic range issues for a vast range of lightness intensities, many tone mapping operators have employed various hypothetical models that simulate the HVS. For example, the retinex theory [22], which reproduces the sensory response to color stimuli by using the HVS, has been implemented in many local tone mapping operators. Jobson et al. [11] introduced a multi-scale center/surround retinex to produce an LDR image similar to human visual perception. This multi-scale retinex was extended by Meylan and Süsstrunk [12] to provide a good color rendition and prevent halo artifacts in the tone mapping process. In addition, Mantiuk et al. [19] introduce a perceptual framework to incorporate the characteristics of a HVS into the gradient attenuating process. They reconstruct the low frequency of the tone-mapped image

* Corresponding author.
E-mail addresses: dhlee@dali.korea.ac.kr (D.-H. Lee), mingfan@dali.korea.ac.kr (M. Fan), swkim@dali.korea.ac.kr (S.-W. Kim), mckang@dali.korea.ac.kr (M.-C. Kang), sjko@korea.ac.kr (S.-J. Ko).

https://doi.org/10.1016/j.image.2018.07.008
Received 13 March 2018; Received in revised form 30 May 2018; Accepted 15 July 2018
Available online 17 July 2018

by adopting the pyramidal contrast representation. However, these HVS-based local tone mapping methods commonly suffer from halo artifacts and require high computational complexity.

Since the Naka–Rushton equation [23], which represents the response of retinal photoreceptors according to the lightness level, was employed by Pattanaik et al. [2] to reproduce the time-dependent visual adaptation of human eyes, a variety of global tone mapping operators with the Naka–Rushton equation have been proposed. For example, Ledda et al. [3] respectively applied the Naka–Rushton equation to rods and cones for modeling the local visual adaptation in the retina. Reinhard et al. [6] extended the Naka–Rushton equation by using a key value, which indicates whether an input HDR image is subjectively light, normal, or dark. In addition, Reinhard and Devlin [7] identified the tone mapping process with the photography, and obtained the chromatic and lightness adaptation of the Naka–Rushton equation from controllable parameters similar to the variable camera settings from photographer. Recently, Ferradans et al. [9] pointed out the importance of cone saturation and combined both the Naka–Rushton equation and the Weber–Fechner law. However, since the curve of the Naka–Rushton equation has a drawback in that it has a symmetric S-shape on semi-log coordinates, tone-mapped LDR images using the Naka–Rushton equation tend to exhibit loss of details of their corresponding HDR images in a bright or dark area.

In this paper, we first introduce a new asymmetric sigmoid curve (ASC) based on the conventional model of retina adaptation. Inspired by the property of the HVS wherein the retinal response curve actually has an asymmetric shape [24,25] and its symmetric property holds only from low to moderate luminance level [26], the proposed ASC additionally includes an asymmetric parameter that determines the curvature of the curve. Then, we present a global tone mapping operator, which determines the asymmetric parameter of the ASC by using the photography technique, called zone system [27]. In addition, a contrast-enhancing tone mapping function is proposed by formulating a bi-criteria optimization problem as a weighted sum of the two objectives: one for preserving the ASC-based tone mapping function and the other for adjusting the slope of the mapping function in terms of the luminance histogram.

The rest of the paper is organized as follows. In Section 2, we introduce an asymmetric sigmoid curve based on the conventional retinal response model. Section 3 describes in detail the proposed global tone mapping approach based on the ASC. Section 4 presents the experimental results. Finally, Section 5 concludes this paper.

2. Proposed asymmetric retinal response model

The Michaelis–Menten equation [28], the conventional response model of the retina adaptation, describes the nonlinear relationship between the typical response of a retinal neuron, R, and the lightness intensity, I, as follows:

$$\frac{R(I)}{R_{\max}} = \frac{I^n}{I^n + \sigma^n}, \tag{1}$$

where σ is a semi-saturation constant that represents the adaptation level and n is a sensitivity parameter that determines the steepness of a function. The parameter $R_{\max}$ is the maximum response, which has a value of generally 1.0 for normalization. The adaptation level, σ, for a given photoreceptor can be thought of as a function of the light intensities that this photoreceptor has been exposed to in the recent past and is computed as the average light reaching the entire field of view under a stationary lighting condition [7]. Note that the response of a retinal neuron becomes half maximum when $I = \sigma$. As shown in Fig. 1(a), this response model has a symmetric S-shape about its midpoint (σ, 0.5) on the semi-log coordinates. In addition, similar to the mechanism of the HVS wherein the photoreceptor adjusts the adaptation to the background lighting condition, the curve of the Michaelis–Menten equation moves from left to right along the horizontal axis as the adaptation level increases. Fig. 1(b) shows that it dramatically compresses the bright and dark area in a scene, whereas the middle range remains invariant as the sensitivity parameter increases.

Although the Naka–Rushton equation, a special case ($n = 1$) of the Michaelis–Menten equation, has been extensively employed in the tone mapping literature, the curve of this retinal response model has a symmetric S-shape on semi-log coordinates [29]. To overcome this limitation, we propose a new ASC, which encompasses both the asymmetric- and the symmetric-shaped curves.

Recently, to find the best-fitting curve from dose–response data, Gottschalk and Dunn [30] employed an asymmetric sigmoid curve, called 5PL function, defined by

$$R(x) = d + \frac{(a-d)}{\left(1 + \left(\frac{x}{c}\right)^n\right)^b}, \tag{2}$$

where x indicates the input data, and a, b, c, d, and n are the five parameters used for determining the shape of the curve of a function. Since the retinal response becomes zero without light, i.e., $R(0) = 0$, we obtain $a = 0$ from (2). Thus, (2) can be rewritten as

$$\frac{R(x)}{d} = 1 - \left(\frac{c^n}{x^n + c^n}\right)^b. \tag{3}$$

When $b = 1$, the 5PL function in (3) is reduced to

$$\frac{R(x)}{d} = \frac{x^n}{x^n + c^n}. \tag{4}$$

Note that when $d = R_{\max}$ and $c = \sigma$, (4) is identical to the Michaelis–Menten equation in (1). From (3) with $d = R_{\max}$ and $c = \sigma$, the proposed ASC can be defined as

$$\frac{R(x)}{R_{\max}} = 1 - \left(\frac{\sigma^n}{x^n + \sigma^n}\right)^b. \tag{5}$$

The ASC has a symmetric S-shape about its midpoint (σ, 0.5) on the semi-log coordinates when $b = 1$; otherwise, it becomes asymmetric. As the parameter σ increases, the ASC shifts from left to right, as shown in Fig. 1(c). Comparing Fig. 1(b) to (d), as the parameter n increases, the ASC has a steep slope near the point (σ, $1–0.5^b$) similar to the curve of the Michaelis–Menten equation.

As mentioned in the previous section, we designed the ASC to obtain the global tone mapping function. Therefore, the difficulty is in determining how to appropriately select the asymmetric parameter, b, depending on the HDR scenes. An image-adaptive parameter estimation method will be explained in the next section.

3. Proposed tone mapping operators

3.1. ASC-based tone mapping operator

The zone system technique [27], which controls the final appearance of a photographic print, is employed to determine the asymmetric parameter, b, in (5) for an input HDR image. The zone system divides a scene into 11 zones on the tonal scale, and each zone is properly matched from pure black to pure white. Among the zones, Zone V represents 18% middle gray and is commonly used as a standard gray card.

In [6], the zone system was employed with the modified version of the Naka–Rushton equation for converting an HDR scene into an LDR image as follows:

$$f(L) = \frac{\alpha L \left(1 + \frac{1}{L_{\text{white}}^2} \cdot \frac{\alpha L}{L_{\text{avg}}}\right)}{L_{\text{avg}} + \alpha L}, \tag{6}$$

where $f(\cdot)$ is a mapping function; α indicates the key value; L and L_{avg} are the luminance and log average luminance of an input HDR image, respectively; and L_{white} denotes the minimum luminance value mapped to pure white, e.g., 255 for an 8-bit LDR image. The luminance of an

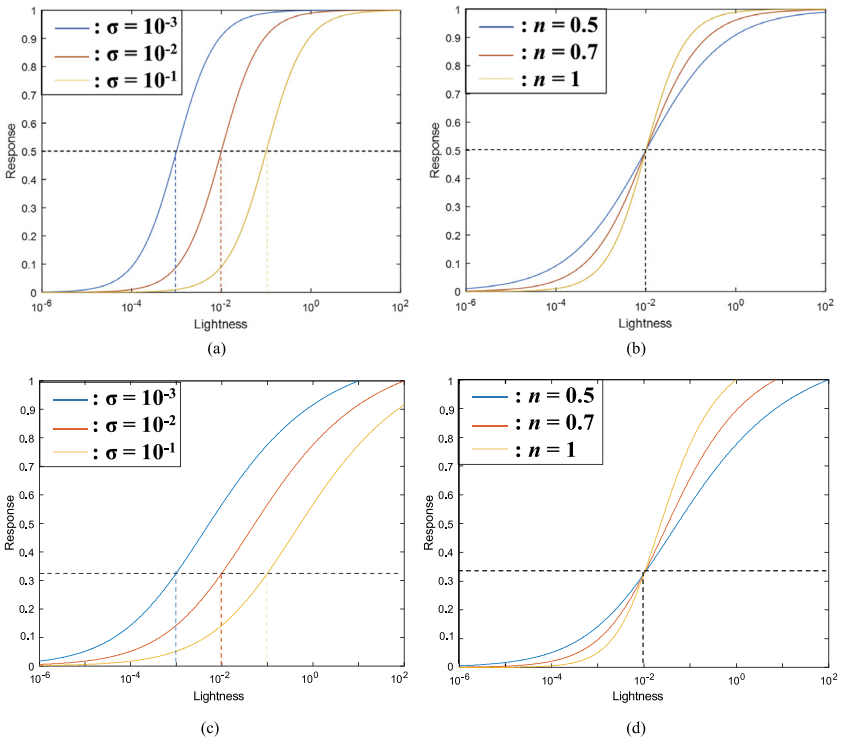

Fig. 1. Response model of the retina as a function of lightness at different σ and n. (a) Curve of the Michaelis–Menten equation with $n = 1$. (b) Curve of the Michaelis–Menten equation with $\sigma = 10^{-2}$. (c) The proposed ASC with $b = 0.5$, $n = 0.5$. (d) The proposed ASC with $b = 0.5$, $\sigma = 10^{-2}$.

HDR image, L, is obtained by weighted averaging the values of three color channels of an input HDR image as follows:

$$L = 0.27 \cdot C_{in}^{R} + 0.67 \cdot C_{in}^{G} + 0.06 \cdot C_{in}^{B}, \tag{7}$$

where C_{in}^{R}, C_{in}^{G}, and C_{in}^{B} denote red, green and blue color channels respectively. In (6), the key value, α, plays a role in determining the appearance of a tone-mapped LDR image because L_{avg} is always mapped to α if $L_{\text{white}} = 1$. In [31], the key value, α, is defined by

$$\alpha = 0.18 \times 4^{k}, \tag{8}$$

$$k = \frac{2\log 2L_{avg} - \log 2L_{\max} - \log 2L_{\min}}{\log 2L_{\max} - \log 2L_{\min}}, \tag{9}$$

where $L_{\max}$ and $L_{\min}$ are respectively the maximum and minimum values of an HDR image, excluding the 1% brightest and dimmest pixels.

In (9), since the range of k is $[-1,1]$, the parameter α is in the range $[0.045, 0.72]$. Here, the important issue is that the proper reflectance of Zone III and Zone VII is approximately equal to 4.5% and 72%, respectively, in the classical zone system. Therefore, we can conclude that the Reinhard global tone mapping curve always passes a point (L_{avg}, α) if $L_{\text{white}} = 1$, and the key value α means the reflectance value between Zone III and Zone VII in terms of k. As shown in Fig. 1(d), the proposed ASC always passes the point (σ, $1–0.5^{b}$). In addition, the adaptation level, σ, is generally computed as a log average luminance, as mentioned in the previous section. Therefore, we set $\sigma = L_{\text{avg}}$ and equate the point (L_{avg}, α) obtained from the zone system with the point (σ, $1–0.5^{b}$) on the ASC. In other words, the asymmetric parameter b is determined from the following equation: $1–0.5^{b} = \alpha$. Finally, the ASC-based proposed tone mapping function, $f_{\text{TM}}(\cdot)$, is obtained by

$$f_{\text{TM}}(L) = 1 - \left(\frac{{L_{\text{avg}}}^{n}}{L^{n} + {L_{\text{avg}}}^{n}}\right)^{b}, \tag{10}$$

$$b = -\log 2\left(1 - 0.18 \times 4^{\frac{2\log 2L_{\text{avg}} - \log 2L_{\max} - \log 2L_{\min}}{\log 2L_{\max} - \log 2L_{\min}}}\right). \tag{11}$$

In a recent work [9], the geometric average between the arithmetic mean and the median of the luminance values represents better the background lightness than the log-average luminance. Therefore, we compute the background intensity: $L_{\text{avg}} = \text{median}^{0.5}\text{mean}^{0.5}$ in (10) and (11).

3.2. Contrast-enhancing tone mapping operator

In this section, we present a method for generating a contrast-enhancing tone mapping function by using both the ASC-based tone mapping function in (10) and the luminance histogram of an input HDR image. Ward et al. [8] first employed the cumulative distribution of a luminance histogram as a global tone mapping function. The resultant tone-mapped LDR image showed an enhanced contrast similar to a histogram-equalized LDR image. However, the histogram-based global tone mapping operator tends to suffer from the loss of details of an HDR image in bright or dark areas [32]. Although the local tone mapping operator can enhance local contrast and visibility of detail, it requires high computational complexity as mentioned in Section 1

To solve this problem, we present an optimization problem with two goals: preserving the shape of the ASC-based tone mapping function described in the previous section and adjusting the slope of the target mapping function, depending on the cumulative distribution function (CDF) of an HDR image. This bi-criteria optimization problem can be formulated as

$$\hat{\mathbf{f}}_{\text{TM}} = \arg\min_{\mathbf{f}} \|\mathbf{f} - \mathbf{f}_{\text{TM}}\|_2^{\,2} + \lambda \|\mathbf{D}\mathbf{f} - \mathbf{D}\mathbf{c}_x\|_2^{\,2}, \tag{12}$$

where $\hat{\mathbf{f}}_{\text{TM}}$ and $\mathbf{f}_{\text{TM}}$ is a vector form of the target mapping function and the discretized ASC-based mapping function, $\mathbf{c}_x$ is the CDF of an input HDR image, λ is a constant that controls the fidelity of $\mathbf{Df}$ to $\mathbf{Dc}_x$, and $\mathbf{D}$ is a bi-diagonal difference matrix given by

$$\mathbf{D} = \begin{bmatrix} 1 & 0 & 0 & \cdots & 0 & 0 & 0 \\ -1 & 1 & 0 & \cdots & 0 & 0 & 0 \\ \vdots & \vdots & \vdots & & \vdots & \vdots & \vdots \\ 0 & 0 & 0 & \cdots & -1 & 1 & 0 \\ 0 & 0 & 0 & \cdots & 0 & -1 & 1 \end{bmatrix}. \tag{13}$$

The discretized ASC-based mapping function, $\widetilde{f}_{\mathrm{TM}}(\cdot)$, is defined as

$$\widetilde{f}_{TM}(i) = f_{TM}\left(\exp(\widetilde{L}_{\min} + i \cdot \frac{\widetilde{L}_{\max} - \widetilde{L}_{\min}}{N-1})\right), \tag{14}$$

where $\widetilde{L}$ is the logarithm of a luminance image, i.e., $\widetilde{L} = \log(L)$, and N is the number of bins of a luminance histogram. In (12), the influence of the gradient term becomes negligible as λ goes to 0 and the optimum mapping function, $\hat{\mathbf{f}}_{\mathrm{TM}}$, becomes $\mathbf{f}_{\mathrm{TM}}$. Moreover, as λ increases, the slope of the target mapping function becomes similar to the slope of the CDF. Therefore, we can control the trade-off between the ASC-based tone mapping operator and the histogram-based tone mapping operator by using λ. The solution of this bi-criterion problem in (12) is

$$\begin{aligned}\hat{\mathbf{f}}_{\mathrm{TM}} &= \left(\mathbf{I} + \lambda \mathbf{D}^T\mathbf{D}\right)^{-1}\left(\mathbf{f}_{TM} + \lambda \mathbf{D}^T\mathbf{D}\mathbf{c}_x\right) \\ &= \mathbf{K}_\lambda\left(\mathbf{f}_{\mathrm{TM}} + \lambda \mathbf{D}^T\mathbf{D}\mathbf{c}_x\right),\end{aligned} \tag{15}$$

where $\mathbf{K}_\lambda = \left(\mathbf{I} + \lambda \mathbf{D}^T\mathbf{D}\right)^{-1}$.

In (12), the slope of the CDF, $\mathbf{D}\mathbf{c}_x$, is equal to the probability distribution function of an input HDR image. In addition, we minimize the difference between the slope of the target mapping curve and $\mathbf{D}\mathbf{c}_x$, instead of the absolute difference. This strategy is useful for only varying the slope of the target mapping curve without the deformation of the shape of an ASC. We will show the effectiveness of the proposed optimization strategy at the end of this section.

Unlike the histogram of an LDR image discretized in [0,255], the luminance values of an HDR image are continuous and need to be discretized. To obtain the histogram of an input HDR image, we represent a histogram with a column vector $\mathbf{h}_x$, whose ith element h_i denotes the number of pixels with $\widetilde{L}$, $\widetilde{L}_{\min} + i \cdot (\widetilde{L}_{\max} - \widetilde{L}_{\min})/(N-1) \le \widetilde{L} < \widetilde{L}_{\min} + (i+1) \cdot (\widetilde{L}_{\max} - \widetilde{L}_{\min})/(N-1)$. The normalized column vector, $\bar{\mathbf{h}}_x$, is then given by

$$\bar{\mathbf{h}}_x = \frac{1}{\mathbf{1}^t\mathbf{h}_x}\mathbf{h}_x. \tag{16}$$

where $\mathbf{1}$ denotes the column vector wherein all elements are 1.

To avoid histogram spikes that cause an over-enhancement problem in tone mapping, we modify $\bar{\mathbf{h}}_x$ by using the smoothness penalty term [33], which reduces the difference of the histogram, i.e., h_{i+1}-h_i, as follows:

$$\mathbf{h}_t = \arg\min_{\mathbf{h}} \left\|\mathbf{h} - \bar{\mathbf{h}}_x\right\|_2{}^2 + \gamma \left\|\mathbf{D}\mathbf{h}\right\|_2{}^2, \tag{17}$$

where $\mathbf{h}_t$ is a target histogram and γ is a smoothness parameter. In (17), $\mathbf{h}_t$ equals to $\bar{\mathbf{h}}_x$ when $\gamma = 0$, and as γ goes to infinity, it converges to the uniformly distributed histogram. The closed form solution of (17) is

$$\begin{aligned}\mathbf{h}_t &= \left(\mathbf{I} + \gamma \mathbf{D}^T\mathbf{D}\right)^{-1}\bar{\mathbf{h}}_x \\ &= \mathbf{K}_\gamma\bar{\mathbf{h}}_x,\end{aligned} \tag{18}$$

where $\mathbf{K}_\gamma = \left(\mathbf{I} + \gamma \mathbf{D}^T\mathbf{D}\right)^{-1}$. The vector form of the smoothed CDF, $\mathbf{c}_t$, is then obtained by

$$\mathbf{c}_t = \mathbf{S}\mathbf{h}_t = \mathbf{S}\mathbf{K}_\gamma\bar{\mathbf{h}}_x, \tag{19}$$

where S is an $N \times N$ lower triangular matrix, an inverse matrix of $\mathbf{D}$, i.e.,

$$\mathbf{S} = \mathbf{D}^{-1} = \begin{bmatrix} 1 & 0 & \cdots & 0 & 0 \\ 1 & 1 & \cdots & 0 & 0 \\ \vdots & \vdots & & \vdots & \vdots \\ 1 & 1 & \cdots & 1 & 0 \\ 1 & 1 & \cdots & 1 & 1 \end{bmatrix}. \tag{20}$$

Finally, by substituting the smoothed CDF, $\mathbf{c}_t$, in (19) into the original CDF, $\mathbf{c}_x$, in (15), we obtain the vector form of the proposed contrast-enhancing tone mapping function, $\widetilde{\mathbf{f}}_{\mathrm{TM}}$, by

$$\widetilde{\mathbf{f}}_{\mathrm{TM}} = \mathbf{K}_\lambda\left(\mathbf{f}_{\mathrm{TM}} + \lambda \mathbf{D}^T\mathbf{K}_\gamma\bar{\mathbf{h}}_x\right). \tag{21}$$

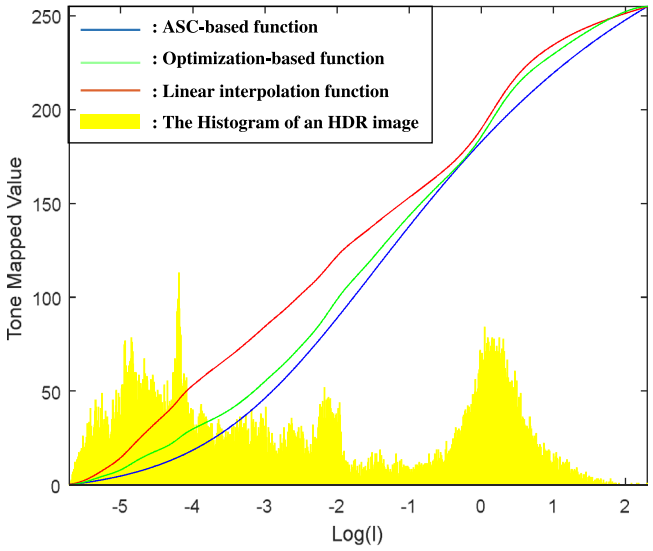

Fig. 2. The three tone mapping functions (the ASC-based function, the optimization-based function, and the interpolation-based function), and the histogram of an HDR image.

In the proposed method, the ASC-based mapping function is combined with the CDF by solving an optimization problem instead of a simple interpolation method. Fig. 2 shows the tone mapping functions using the optimization strategy and the interpolation method. The interpolation-based tone mapping function is obtained by

$$\hat{\mathbf{f}}_{\mathrm{TM}} = \lambda'\mathbf{f}_{\mathrm{TM}} + (1-\lambda')\mathbf{c}_x, \tag{22}$$

where λ' is a weight coefficient. As mentioned before, the proposed optimization strategy well preserves the shape of the ASC-based tone mapping curve and properly adjusts the slope of the target mapping curve. As shown in Fig. 2, the shape of the optimization-based curve is similar to that of the ASC, and the slope of the curve depends on the histogram of an input HDR image. Meanwhile, the shape of the interpolation-based curve heavily depends on the CDF and thus that of the ASC cannot be preserved.

4. Experimental results

4.1. Implementation

In this section, the numerous experiments were implemented to validate the performance of the proposed tone mapping functions, $\mathbf{f}_{\mathrm{TM}}$ and $\widetilde{\mathbf{f}}_{\mathrm{TM}}$.

Prior to the evaluation of the proposed method, the linear formula for color correction [34] was applied on each color channel to color treatment in tone mapping as follows:

$$C_{\mathrm{out}} = \left(\left(\frac{C_{\mathrm{in}}}{L} - 1\right)s + 1\right)L_{\mathrm{out}}, \tag{23}$$

where C denotes one of the color channels (red, green, and blue), L_{out} is the output luminance of the proposed tone mapping operator, and s is the control parameter for color saturation.

In the experiments, 40 test images were selected from two HDR image datasets, namely, MPI and sIBL. Note that the MPI dataset has been widely used in HDR tone mapping, whereas the sIBL dataset includes the latest HDR images, which mainly cover outdoor scenes with ultra-high resolution, as shown in Fig. 3.

Fig. 3. Results of the proposed contrast-enhancing tone mapping method for several images from two HDR datasets. (a) MPI dataset; (b) sIBL dataset.

Fig. 4. Comparison of the ASC-based tone-mapped images via different values of b. (a) $b = 1$ (symmetric function), (b) $b = 0.5$, (c) $b = 0.3$, and (d) b calculated using (10) (top row: $b = 0.1706$; bottom row: $b = 0.7461$).

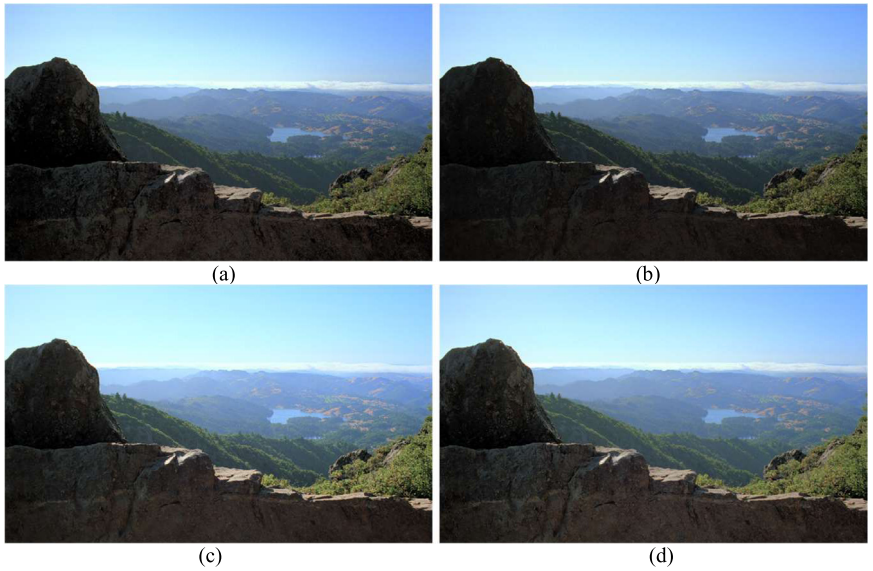

Fig. 5. Comparison of the contrast-enhancing global tone mapping results with varying N. From (a) to (d): $N = 0$, 300, 1000, and 3000.

4.2. Subjective evaluation

Fig. 4 shows the results of the proposed ASC-based tone mapping method with different values of b in (10). For tone mapping, the parameters were set to $n = 1$. As shown in Fig. 4(a), the symmetric version of the proposed tone mapping function ($b = 1$) tends to preserve fine details in the dark region and remove textures in the bright region. As b decreases, the tone-mapped results become darker as shown in Fig. 4(b) and (c). Therefore, the asymmetric parameter b has a significant effect on the image quality of a tone-mapped LDR image. In Fig. 4(d), the parameter b calculated using (10) gives a good trade-off between the preservation of details in the bright region and the dark region of the resultant images.

Unlike the histogram of the LDR image with 256 quantized levels, the luminance values of the HDR image are continuous, and the number of

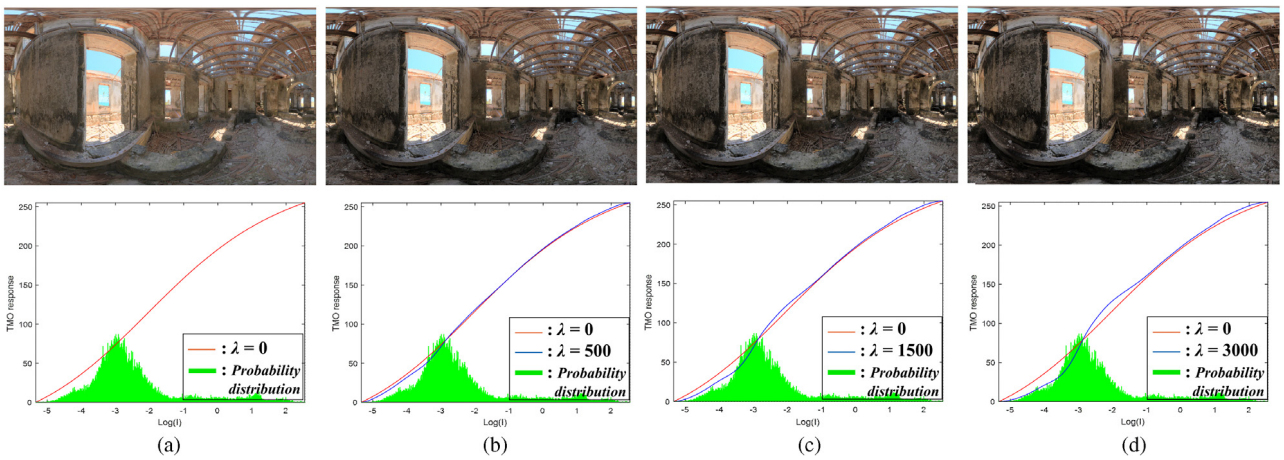

Fig. 6. Comparison of the contrast-enhancing global tone mapping curves and tone-mapped images with varying λ. From (a) to (d): $\lambda = 0$, 500, 1500, and 3000.

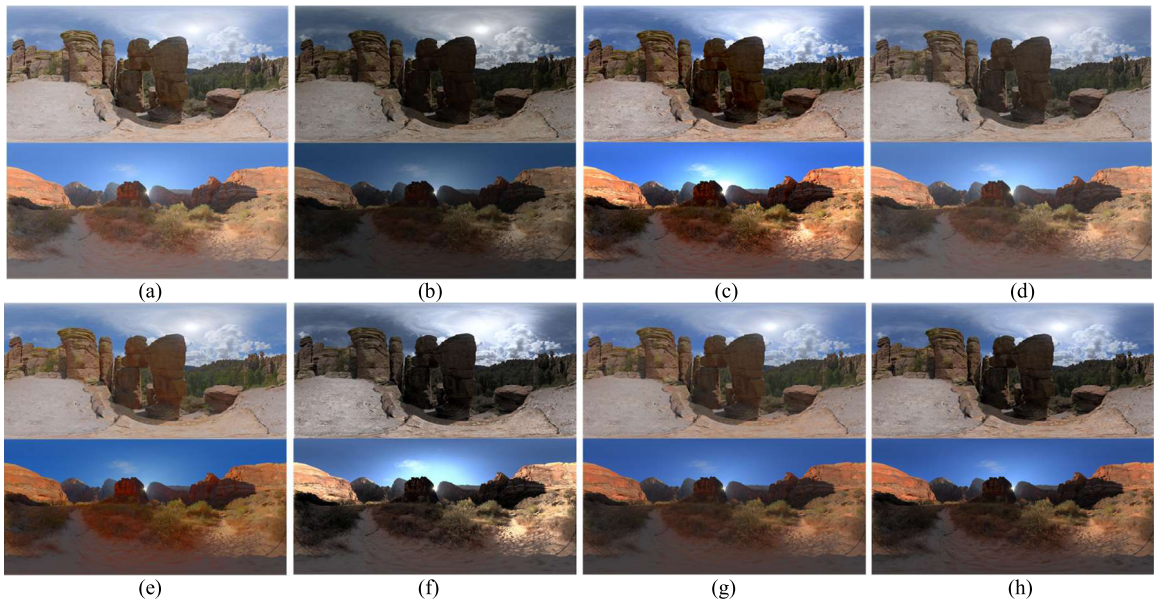

Fig. 7. Resultant tone-mapped LDR images (iSBL dataset) for (a) Drago et al. [4]; (b) Ferradans's et al. [9] (global method); (c) Mantiuk et al. [5]; (d) Reinhard et al. [6]; (e) Reinhard and Devlin [7]; (f) Ward et al. [8]; (g) the proposed ASC-based tone mapping method.; and (h) the proposed contrast-enhancing tone mapping method.

histogram bins of the HDR image, N, affects the quality of our contrast-enhancing tone mapping results. Fig. 5 shows the results of the proposed ASC-based tone mapping method for different values of N in (14). Since the smaller N compresses more HDR information in the histogram generating process, Fig. 5(a) and (b) show that the results obtained by using the smaller N exhibit more loss of details in bright and dark area. Otherwise, the tone mapping operator using the larger N generates visually plausible image details while needs the high computational complexity. Since there is no significant difference between the tone-mapped result with $N = 1000$ and the result with $N = 3000$ as shown in Fig. 5(c) and (d), we set $N = 1000$ for all experiments.

Fig. 6 shows tone-mapped LDR images using the proposed contrast-enhancing tone mapping method with varying λ. As mentioned in Section 3.2, the parameter λ controls the influence of the luminance histogram in the tone mapping process. As λ increases, the slope of the tone mapping curve near the large probability region becomes steeper and the global contrast of the tone-mapped image also becomes markedly enhanced. In the experiments, the parameters λ and γ were empirically determined to be 400, and 50, respectively.

For the performance comparison with the proposed method, other state-of-the art global tone mapping methods were utilized such as Drago's method [4], Mantiuk's method [5], two Reinhard's methods [6] [7], Ward's method [8], and Ferradans's method [9]. Fig. 7 shows the results of our two tone mapping methods and the conventional global tone mapping methods for the sIBL dataset. In the experiments, the tone-mapped results based on the Naka–Rushton equation were shown in Fig. 7(d) and (e). Although the results had sufficient details in dark region, they also appeared with low contrast. Among the conventional methods, Mantiuk's method [5] had the best performance in preserving the global contrast. However, the poor visibility of the image details in the bright and dim regions could be observed, as shown in Fig. 7(c). In contrast, the important fine details and textures of an input HDR image were well presented in the results for the proposed ASC-based tone mapping method, as shown in Fig. 7(g). In Fig. 7(h), the proposed contrast-enhancing tone mapping method not only preserved the image details but also enhanced the global contrast of the tone-mapped LDR image. This tendency is also clearly shown in Fig. 8, which used the MPI dataset.

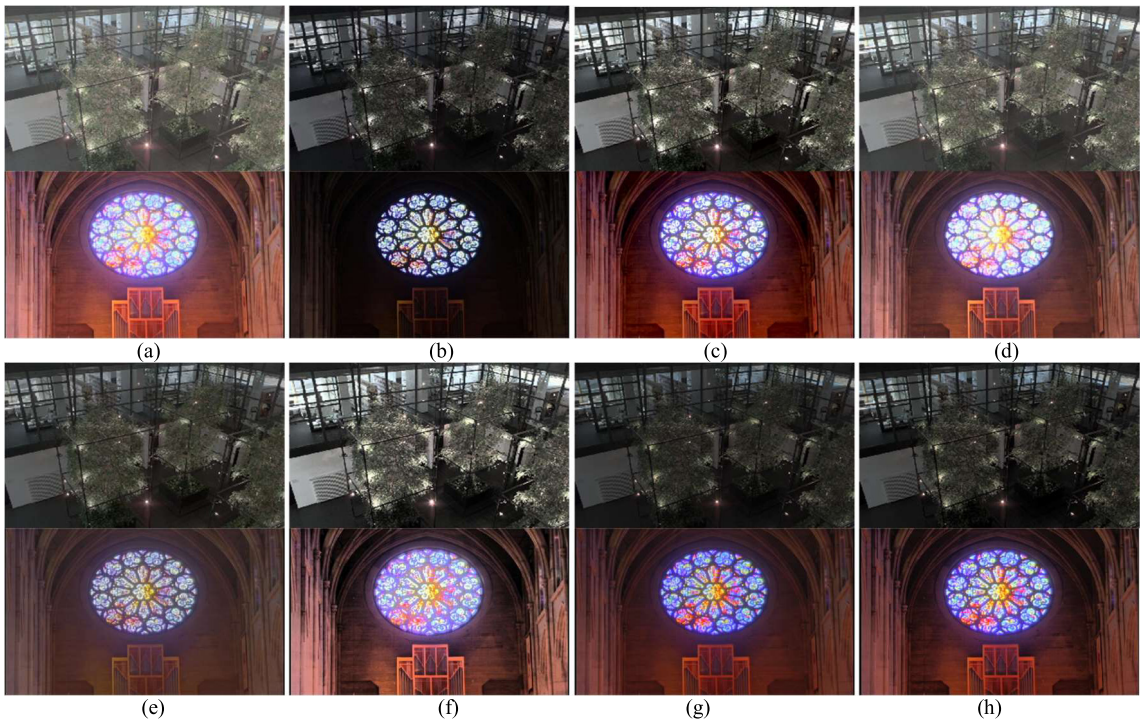

Fig. 8. Resultant tone-mapped LDR images (MPI dataset) for (a) Drago et al. [4]; (b) Ferradans's et al. [9] (global method); (c) Mantiuk et al. [5]; (d) Reinhard et al. [6]; (e) Reinhard and Devlin [7]; (f) Ward et al. [8]; (g) the proposed ASC-based tone mapping method.; and (h) the proposed contrast-enhancing tone mapping method.

4.3. Objective evaluation

For an objective evaluation of the tone-mapped results, the two quantitative quality assessment methods were employed. The first assessment method [35] used the two input images, one for an input HDR image as the reference image, and the other for a tone-mapped LDR image as the test image. The assessment result included a distortion map, which represented the contrast distortion error for each pixel. The gray, green, red, and blue color of the distortion map indicated no distortion, loss of visible contrast, contrast reversal, and amplification of contrast, respectively. In addition, each color density meant the magnitude of error. In Fig. 9, we demonstrate the tone-mapped LDR images and distortion maps generated using the two proposed tone mapping operators and the conventional methods. As shown in Fig. 9(g) and (h), both of the proposed tone mapping methods produced less distortion than the other methods.

For an analysis of the numerical errors, we extracted the error values for each pixel from the 40 tone-mapped LDR images, which contained 20 sIBL images and 20 MPI images, and computed the averages, as shown in Table 1. The result of the method with the best performance is in boldface font, and the second one is in italics. Except for the categories about the loss of contrast, the two proposed methods outperformed the other tone mapping methods. In Table 1, the Ward's method relatively resulted in lower loss and higher reversal and an amplification of the contrast compared to those of other conventional methods. In addition, the contrast-enhancing tone mapping operator created a few more errors in amplification and reversal categories compared with the ASC-based tone mapping operator. Since the tone-mapped results of these two methods commonly exhibited enhanced contrast in Figs. 7 and 8, we can infer that the tone mapping operator with a luminance histogram enhances the global contrast while causing an error in the contrast reverse and amplification.

In the second experiment, the tone-mapped image quality index (TMQI) [20] consisting of a local structural fidelity measure and a statistical naturalness measure was employed. The metric gives an overall performance score between [0, 1], where the higher score indicates the better performance. For fair comparison, we used the same HDR datasets in first experiment and computed three averaged quality scores (structural fidelity, statistical naturalness, and overall quality) and its standard deviations. The results are listed in Table 2. Although the Mantiuk's method [5] performs slightly better than the proposed contrast-enhancing tone mapping method in terms of the structural fidelity, the proposed method outperformed the Mantiuk's method in terms of the statistical naturalness and overall performance. In addition, the standard deviations in Table 2 indicate that each quality score of the proposed contrast-enhancing method tend to be close the averaged quality score.

Tone mapped results using the proposed contrast-enhancing method obtain the high scores for various HDR images. Note that, this tendency was clearly seen in Figs. 7 and 8, where the tone-mapped LDR images from the proposed contrast-enhancing method not only preserves local details but also shows better visual quality as compared with the other tone mapping methods.

5. Conclusion

In this paper, we introduced a new asymmetric sigmoid curve (ASC) based on the human visual system wherein the retinal response curve has an asymmetric shape. Then, we proposed two global tone mapping operators using the ASC. The first one employs the zone system to determine the curvature of the mapping curve depending on an HDR image. The second one enhances the global contrast of the tone-mapped LDR image by formulating a bi-criteria optimization problem with the luminance histogram of an HDR image. Since an optimal solution of this problem can be computed in closed form, it requires low computational complexity. The proposed tone mapping operators were evaluated using two quantitative quality assessment methods and showed high performance to previous approaches.

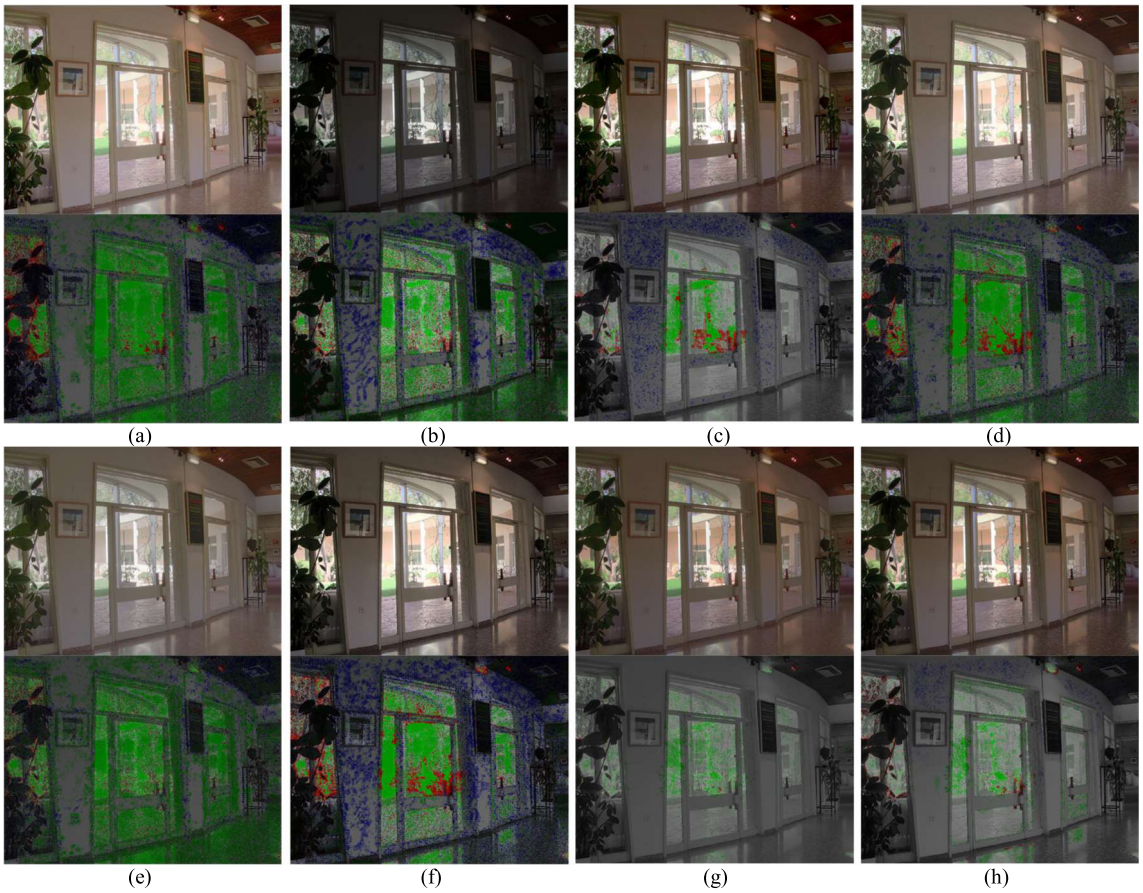

Fig. 9. Comparison of the global tone mapping operators. Tone-mapped LDR images (top row) and distortion maps (bottom row) for (a) Drago et al. [4]; (b) Ferradans's et al. [9] (global method); (c) Mantiuk et al. [5]; (d) Reinhard et al. [6]; (e) Reinhard and Devlin [7]; (f) Ward et al. [8]; (g) the proposed ASC-based tone mapping method.; and (h) the proposed contrast-enhancing tone mapping method.

Table 1
Error percentages computed with Aydin et al. [35], averaged over 40 tone-mapped LDR images.

Method	Loss	Reverse	Amplification	Total
Drago's method [4]	33.92	5.80	2.86	42.58
Ferradans's method [9]	25.10	5.00	4.24	34.34
Mantiuk's method [5]	**5.18**	3.26	1.62	*10.06*
Reinhard's method [6] (2002)	26.35	6.28	3.18	35.81
Reinhard's method [7] (2005)	30.31	3.32	1.94	35.57
Ward's method [8]	16.74	7.96	11.23	35.93
Proposed method 1 (ASC-based method)	7.96	**1.35**	**0.10**	**9.41**
Proposed method 2 (Contrast-enhancing method)	*7.62*	*2.63*	*0.75*	11.00

Table 2
Quality scores computed with TMQI [20], averaged over 40 tone-mapped LDR images.

Method	Structural fidelity (std)	Naturalness (std)	Overall quality (std)
Drago's method [4]	0.831 (0.072)	0.467 (0.292)	0.867 (0.066)
Ferradans's method [9]	0.820 (0.090)	0.382 (0.135)	0.781 (0.047)
Mantiuk's method [5]	*0.890* (0.062)	0.436 (0.190)	*0.881* (0.042)
Reinhard's method [6] (2002)	0.838 (0.071)	*0.459* (0.254)	0.869 (0.060)
Reinhard's method [7] (2005)	0.816 (0.087)	0.237 (0.205)	0.818 (0.060)
Ward's method [8]	0.868 (0.087)	0.381 (0.258)	0.860 (0.067)
Proposed method 1 (ASC-based method)	0.856 (0.077)	0.365 (0.245)	0.856 (0.058)
Proposed method 2 (Contrast-enhancing method)	**0.893** (0.053)	**0.471** (0.240)	**0.886** (0.047)

Acknowledgment

This work was supported by Institute for Information & communications Technology Promotion (IITP) grant funded by the Korea government (MSIT) (2017-0-00250, Intelligent Defense Boundary Surveillance Technology Using Collaborative Reinforced Learning of Embedded Edge Camera and Image Analysis).

References

[1] E. Reinhard, G. Ward, S. Pattanaik, P. Debevec, High Dynamic Range Imaging: Acquisition, Display and Image-Based Lighting, Morgan Kaufmann Publisher, 2005.
[2] S.N. Pattanaik, J. Tumblin, H. Yee, D.P. Greenberg, Time-dependent visual adaptation for fast realistic image display, in: Proc. Comput. Graph. Interact. Tech. 2000, pp. 47–54.
[3] P. Ledda, L.P. Santos, A. Chalmers, A local model of eye adaptation for high dynamic range images, Assoc. Comput. Mach. 1 (2004) 151–161.
[4] F. Drago, K. Myszkowski, T. Annen, N. Chiba, Adaptive logarithmic mapping for displaying high contrast scenes, Comput. Graph. Forum 22 (3) (2003) 419–426.
[5] R. Mantiuk, S. Daly, L. Kerofsky, Display adaptive tone mapping, ACM Trans. Graph. 27 (3) (2008) 68–78.
[6] E. Reinhard, M. Stark, P. Shirley, J. Ferwerda, Photographic tone reproduction for digital images, ACM Trans. Graph. 21 (3) (2002) 267–276.
[7] E. Reinhard, K. Devlin, Dynamic range reduction inspired by photoreceptor physiology, IEEE Trans. Vis. Comput. Graphics 11 (1) (2005) 13–24.
[8] G.W. Larson, H. Rushmeier, C. Piatko, A visibility matching tone reproduction operator for high dynamic range scenes, IEEE Trans. Vis. Comput. Graphics 3 (4) (1997) 291–306.
[9] S. Ferradans, M. Bertalmio, E. Provenzi, V. Caselles, An analysis of visual adaptation and contrast perception for tone mapping, IEEE Trans. Pattern Anal. Mach. Intell. 33 (10) (2011) 2002–2012.
[10] C. Schlick, Quantization techniques for the visualization of high dynamic range pictures, in: Proc. P.R.T. Eurographics, 1994, pp. 7–20.
[11] D.J. Jobson, Z. Rahman, G.a Woodell, Properties and performance of a center/surround retinex, IEEE Trans. Image Process. 6 (3) (1997) 451–462.
[12] L. Meylan, S. Süsstrunk, High dynamic range image rendering with a Retinex-based adaptive filter, IEEE Trans. Image Process. 15 (9) (2006) 2820–2830.
[13] T. Horiuchi, S. Tominaga, HDR image quality enhancement based on spatially variant retinal response, EURASIP J. Image Video Process. (2010) 1–11.
[14] J.H. Kim, H. Kim, S. Ko, New visualization method for high dynamic range images in low dynamic range devices, Opt. Eng. 50 (10) (2011) 107005-1-7.
[15] J. Duan, M. Bressan, C. Dance, G. Qiu, Tone-mapping high dynamic range images by novel histogram adjustment, Pattern Recognit. 43 (5) (2010) 1847–1862.
[16] B. Gu, W. Li, M. Zhu, M. Wang, Local edge-preserving multiscale decomposition for high dynamic range image tone mapping, IEEE Trans. Image Process. 22 (1) (2013) 70–79.
[17] F. Durand, J. Dorsey, Fast bilateral filtering for the display of high-dynamic-range images, ACM Trans. Graph. 21 (3) (2002) 257–266.
[18] R. Fattal, D. Lischinski, M. Werman, Gradient domain high dynamic range compression, in: Proc. A.C.C.G. SIGGRAPH, 2002, pp. 249–256.
[19] R. Mantiuk, K. Myszkowski, H.-P. Seidel, A perceptual framework for contrast processing of high dynamic range images, ACM Trans. Appl. Percept. 3 (3) (2006) 286–308.
[20] H. Yeganeh, Z. Wang, Objective quality assessment of tone-mapped images, IEEE Trans. Image Process. 22 (2) (2013) 657–667.
[21] Y. Salih, W. bt. Md-Esa, A.S. Malik, N. Saad, Tone mapping of HDR images: A review, in: Int. Conf. Intell. Adv. Syst. Vol. 1, 2012, pp. 368–373.
[22] E. Land, The retinex theory of color vision, Sci. Am. 237 (6) (1977) 108–128.
[23] K.I. Naka, W.A. Rushton, S-potentials from colour units in the retina of fish (Cyprinidae), J. Physiol. 185 (3) (1966) 536–555.
[24] N.S. Peachey, K.R. Alexander, G.A. Fishman, The luminance-response function of the dark-adapted human electroretinogram, Vision Res. 29 (3) (1989) 263–270.
[25] S. Grossberg, F. Kelly, Neural dynamics of binocular brightness perception, Vision Res. 39 (22) (1999) 3796–3816.
[26] O.H. Shade, Optical and photoelectric analog of the eye, J. Opt. Soc. Amer. 46 (9) (1956) 721–739.
[27] A. Adams, The Zone System revisited. Part I, Pop. Photogr. 88 (11) (1981) 99–149.
[28] L. Michaelis, M.L. Menten, Die Kinetik der Invertinwerkung, Bochemische Z. (1913) 49.
[29] R. Shapley, R. Shapley, C. Enroth-cugell, C. Enroth-cugell, Visual adaptation and retinal gain control, Prog. Retin. Res. 3 (1984) 263–346.
[30] P.G. Gottschalk, J.R. Dunn, The five-parameter logistic: A characterization and comparison with the four-parameter logistic, Anal. Biochem. 343 (1) (2005) 54–65.
[31] E. Reinhard, Parameter estimation for photographic tone reproduction, J. Graph. Tools 7 (1) (2002) 45–51.
[32] J. Duan, M. Bressan, C. Dance, G. Qiu, Tone-mapping high dynamic range images by novel histogram adjustment, Pattern Recognit. 43 (5) (2010) 1847–1862.
[33] T. Arici, S. Dikbas, Y. Altunbasak, A histogram modification framework and its application for image contrast enhancement, IEEE Trans. Image Process. 18 (9) (2009) 1921–1935.
[34] R. Mantiuk, A. Tomaszewska, W. Heidrich, Color correction for tone mapping, Comput. Graph. Forum 28 (2) (2009) 193–202.
[35] T.O. Aydin, R. Mantiuk, K. Myszkowski, H.-P. Seidel, Dynamic range independent image quality assessment, ACM Trans. Graph. 27 (3) (2008) 69–73.

Dae-Hong Lee received a B.S. degree in Electrical Engineering from Korea University in 2011. He is currently pursuing a Ph.D. degree in Electrical Engineering at Korea University , Seoul, Republic of Korea His research interests are in the area of HDR imaging and computer vision.

Ming Fan received the B.S. degree in Electronics Engineering from Dongguk University in 2014. He entered the Computer Vision and Image Processing Lab. in the Department of Electronic Engineering of Korea University. He is now a Ph.D. candidate at Korea University. His interests are in the area of image processing, and computer vision.

Seung-Wook Kim received his B.S. in Electronics Engineering from Korea University, Seoul, Rep. of Korea, in 2012. He entered the Computer Vision and Image Processing Lab. in the Department of Electrical Engineering of Korea University in March 2012, and is currently pursuing a Ph.D. degree. His research interests are in the areas of image processing and computer vision.

Mun-Cheon Kang received the B.S. degree from Electrical Engineering at Korea University, Seoul, Korea, in 2011. He is currently pursuing Ph.D. degree in Electrical Engineering from Korea University, Seoul, Republic of Korea His research interests are in the areas of human–machine interaction, gaze tracking, and 3-D vision.

Sung-Jea Ko (M'88-SM'97-F'12) received his Ph.D. degree in 1988 and his M.S. degree in 1986, both in Electrical and Computer Engineering, from State University of New York at Buffalo, and his B.S. degree in Electronic Engineering at Korea University in 1980. In 1992, he joined the Department of Electronic Engineering at Korea University where he is currently a Professor. From 1988 to 1992, he was an Assistant Professor in the Department of Electrical and Computer Engineering at the University of Michigan-Dearborn. He has published over 180 international journal articles. He also holds over 60 registered patents in fields such as video signal processing, computer vision, and multimedia communications.

He is the 1999 Recipient of the LG Research Award. He received the Hae-Dong best paper award from the Institute of Electronics and Information Engineers (IEIE) (1997), the best paper award from the IEEE Asia Pacific Conference on Circuits and Systems (1996), a research excellence award from Korea University (2004), and a technical achievement award from the IEEE Consumer Electronics (CE) Society (2012). He received a 15-year service award from the TPC of ICCE in 2014 and the Chester Sall award from the IEEE CE Society in 2017. He has served as the General Chairman of ITC-CSCC 2012 and the General Chairman of IEICE 2013. He is a member of the editorial board of the IEEE Transactions on Consumer Electronics. He is a distinguished lecturer of the IEEE. He was the President of the IEIE in 2013 and the Vice-President of the IEEE CE Society from 2013 to 2016. He is a Fellow of the IEEE (2012) and a Fellow of the Institution of Engineering and Technology (IET) (2000).